

Exploiting synergies between sustainable ammonia and nitric acid production: A techno-economic assessment

Nicole Carina Neumann^{a,*}, David Baumstark^a, Pablo López Martínez^{a,b}, Nathalie Monnerie^a, Martin Roeb^a

^a German Aerospace Center, Institute of Future Fuels, Linder Höhe, Köln, 51147, Germany

^b Technical University of Denmark, Process and Systems Engineering Centre, Søtofts Plad, Kongens Lyngby, 2800, Denmark

ARTICLE INFO

Handling Editor: Jin-Kuk Kim

Keywords:

Nitric acid
Process simulation
Solar energy
Ostwald process
Explosion limits
Oxygen injection

ABSTRACT

The decarbonization of the fertilizer industry is an important step towards a climate-neutral society. Nitric acid produced via the Ostwald process is a key precursor to nitrogen-based fertilizers, with the production of ammonia representing an important intermediate step. This work focuses on the search for synergies between the sustainable production of ammonia feedstocks – hydrogen and nitrogen – and nitric acid production in the Ostwald process: Oxygen a by-product of sustainable hydrogen and nitrogen production was considered for injection in the Ostwald process at 4 points. A techno-economic assessment was performed to identify the technical and economic potential of this air enrichment. In addition, the safety implications of applying a higher oxygen concentration in the ammonia combustion step of the Ostwald process was evaluated based on explosion limit simulations. The techno-economic assessment was based on a mono-pressure nitric acid plant with a plant capacity of 700 t/d of pure nitric acid at a concentration of 60 wt% in water. The investigations of injecting oxygen at four different points of the plant show that daily nitric acid production can be increased by 0.31% and final NO_x concentration of the absorption column can be reduced by up to 43.6% by enriching the main air pipeline with oxygen. Optimal oxygen injection could reduce the capital costs by 0.41 M€. Nevertheless, the operating costs dominated the final cash flow analysis with ammonia costs accounting for ca. 60% of the total operating costs. The CO₂ price would need to increase to at least 233 €/t to compensate for the higher green ammonia price and equalize the minimum selling price. As the oxygen injection at the main air line comes with safety risks due to the ammonia explosion limits, we evaluated the effect of O₂-enrichment on the explosion limits of NH₃-O₂-N₂ mixtures. The foreseen oxygen enrichment reduced the lower explosion limit only marginally. For a medium pressure plant at 5.8 bar the lower explosion limit is reduced to 10.3% for the highest considered oxygen injection case, which is close to the applied ammonia concentration.

1. Introduction

The world's population growth to 8 billion would not have been possible without the development of the fertilizer industry (Randive et al., 2021). Nitric acid, along with ammonia, constitutes an important feedstock for the production of nitrogen-based fertilizers due to its high nitrogen content (15.5% to 34.5%) and its rapid release as a major plant nutrient. Thus, around 80% of the global nitric acid production is used to produce fertilizers (Smil, 2004).

Despite the importance of nitrogen-based fertilizers for modern society, their production and use have considerable impacts on the environment (Kniel et al., 1996). In fact, the production and transportation of N-based fertilizers account for 0.9% of global greenhouse gas (GHG) emissions (Menegat et al., 2022). Thus, pathways towards green

ammonia production are currently investigated. These pathways need to include both green hydrogen production, e.g. by electrolysis or solar-powered thermochemical cycles (Budama et al., 2022; Vieten et al., 2020; Rosenstiel et al., 2021), and the provision of very pure nitrogen with oxygen impurities below 10 ppm, in order to avoid catalyst deactivation in the subsequent Haber–Bosch process (Moghaddam and Krewer, 2020). The combination of a pressure-swing adsorption unit with thermochemical air separation based on the non-stoichiometric redox reaction of perovskites presents one promising option to provide such pure nitrogen in an energy-efficient way for large range of plant scales (Klaas et al., 2023). This novel process would allow for ammonia being solely produced with water, air and solar energy.

* Corresponding author.

E-mail address: nicole.neumann@dlr.de (N.C. Neumann).

<https://doi.org/10.1016/j.jclepro.2024.140740>

Received 6 November 2023; Received in revised form 30 December 2023; Accepted 11 January 2024

Available online 19 January 2024

0959-6526/© 2024 The Authors. Published by Elsevier Ltd. This is an open access article under the CC BY license (<http://creativecommons.org/licenses/by/4.0/>).

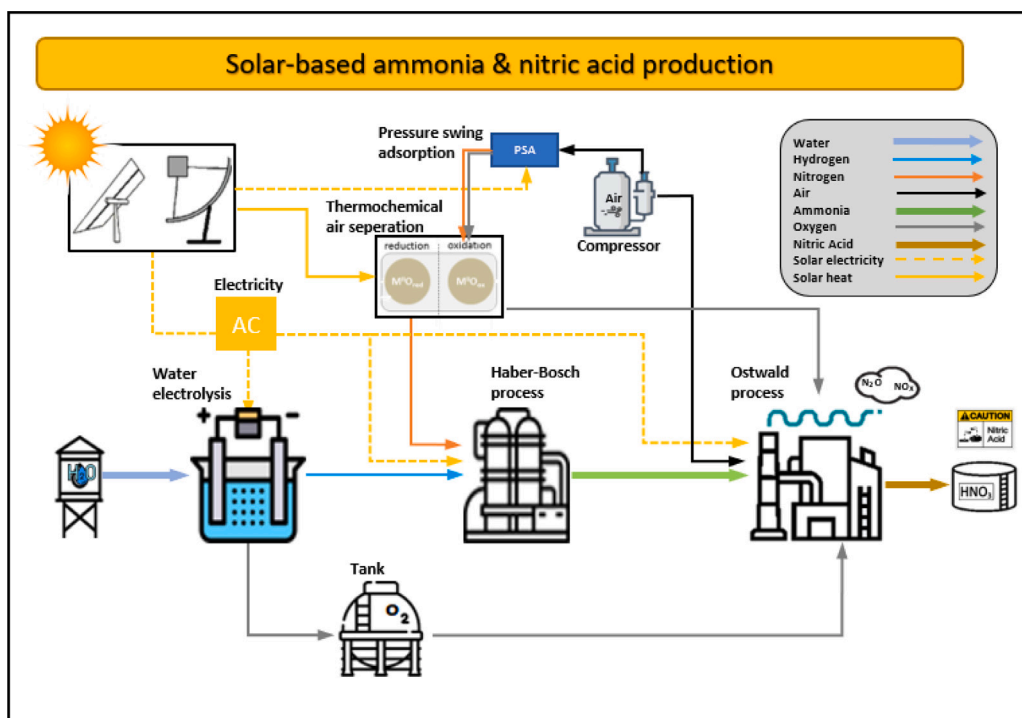


Fig. 1. Pathways for a solar-based ammonia & nitric acid production.

Oxygen is a natural by-product of both hydrogen production and the separation of nitrogen from the air. This surplus oxygen can be integrated into existing nitric acid plants at several points of the process to increase nitric acid production and reduce NO_x emissions or allow a reduction in the capital cost of new nitric acid plants (Wagner and Plains, 2003). More specifically, oxygen-enriched air in the ammonia combustion step could maximize the catalytic combustion of ammonia, reduce the amount of inert gas (nitrogen) in the system, and thus compression costs. In addition, the NO_x gases concentration in the tail-gas can be reduced due to improved conversion rates of the gaseous nitrous oxides, and the bleaching process could be boosted to increase the nitric acid strength and quality of the final product (Echegaray et al., 2000; Wagner and Plains, 2003; Bhatia et al., 1997; Powell, 1975).

Although many patents hint at this beneficial integration of oxygen to the conventional Ostwald process, no study identified the techno-economic potential of a sustainable process chain including also a safety analysis regarding the use of surplus oxygen in ammonia combustion. Thus, this work focuses on the synergies between solar-powered ammonia production and the downstream processing into nitric acid in the Ostwald process. A schematic of the overall process chain is given in Fig. 1. The motivation is to produce green ammonia using solar technologies for the required energy, as well as, the required hydrogen and nitrogen production. A specific focus is put on the effect of integrating the surplus oxygen obtained as by-product from the hydrogen and nitrogen production into the Ostwald process as oxygen-enriched air.

Within this study, the Ostwald process is modeled in Aspen Plus[®] as a mono-pressure (5.8 bar) plant with a capacity of 700 t/d nitric acid. We defined four scenarios of different oxygen injection points – before the ammonia burner, before the cooler, before the absorption tower and before the bleacher column – to identify the effect on nitric acid strength, production rate and NO_x emissions. The injection of surplus oxygen prior to ammonia combustion is limited by the lower explosion limit of ammonia–oxygen mixtures in nitrogen (Haynes, 2019). Therefore, the influence of oxygen enrichment on the explosion limit of ammonia is also analyzed in this work. Finally, we assessed the

economics of the most promising oxygen-injection scenario in comparison to conventional nitric acid production with and without renewable energy supply.

2. Methodology

2.1. Process simulation

The nitric acid synthesis process is known as the Ostwald process. The process consists of three main steps: the ammonia combustion, the oxidation of nitric oxide into nitrogen dioxide and dinitrogen tetroxide and the absorption of the formed nitrogen oxides in water. Nitric acid plants are typically divided into mono-pressure and dual-pressure plants. Mono-pressure nitric acid plants are more suitable in locations with lower energy costs and shorter depreciation periods. Dual-pressure processes are preferably used when large capacities are needed, since it combines the favorable economics of medium pressure combustion with efficiency of high-pressure absorption (Thiemann et al., 2000). A medium size mono-pressure nitric acid plant is selected for the simulation in Aspen Plus[®] based on an initial sizing of the process depicted in Fig. 1 in which a concentrated solar power plant provides electricity and heat. Thus, the nitric acid plant is designed to operate at 5.8 bar with a capacity fixed to 700 t/d of nitric acid (100 wt%) which is equivalent to 1166.67 t/d of product at a nitric acid concentration of 60 wt%. This acid concentration is suitable for fertilizer production (Clarke et al., 2005).

The process flowsheet, including the operating conditions, is shown in Fig. 2. Liquid ammonia is first vaporized (E-101) and overheated (E-102) at 150 °C, before being mixed with the air stream. Filtered atmospheric air passes through a three-stages compressor train (C-101) to remove air moisture and achieve the design pressure of 5.8 bar. This air-stream is split into two streams: a primary stream goes to the ammonia-air mixer and a secondary stream goes to the bleaching column (T-102). The ammonia-air mixture is preheated to 200 °C upstream of the ammonia burner (R-101). Ammonia and air are combusted while crossing through a Pt-Rh catalytic gauze. During the

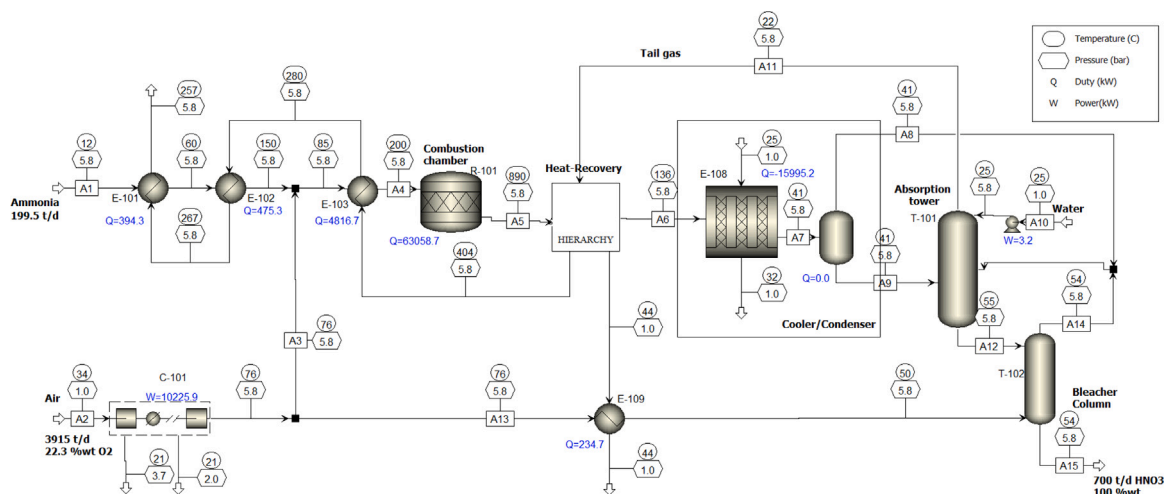


Fig. 2. Aspen Plus® flowsheet of simulated nitric acid plant.

catalytic combustion, 63.1 MW of heat are released and a gas stream composed of nitrogen oxides, nitrogen and oxygen is produced.

During the heat recovery, nitric oxide is first oxidized to nitric dioxide and secondly dimerized to form dinitrogen tetroxide. The detailed heat exchanger specifications and the modeling approach can be found in Appendix A. Furthermore, the NO_x gas stream is partially condensed in a cooler-condenser (E-108) with the help of cooling-water. A high quantity of weak nitric acid is formed at the bottom and sent to the lower-middle part of the absorption column (T-101). On the other side, the remain gas stream is mixed with the air leaving the bleaching column (T-102) and sent to the bottom of the absorption column. The NO_x gas stream is counter-currently contacted with process water entering at the top of the column. The absorption process results in the required nitric acid strength being achieved at the bottom of the column. Finally, the liquid acid is transported to the bleaching column to be bleached with secondary air. The NO_x gases leaving at the top of the absorption column are transported to a series of gas-gas heat exchangers. Afterwards, they are treated in a NO_x capture system before the exhaust gas is discharged into the atmosphere. Overall 199.5 t/d of ammonia, 3915.5 t/d of air and 243.6 t/d of process water are needed to produce 700 t/d of pure nitric acid.

Thermodynamic models

The electrolyte nonrandom two-liquid (ELECNRTL) thermodynamic model provides an accurate description of the aqueous nitric acid system and is thus selected for the absorption step (Mock et al., 1986). Nitric acid is a strong acid that in presence of water is dissociated into hydronium and nitrate ions. Therefore, the presence of ions in the liquid phase requires non-ideal solution thermodynamics, which are covered by ELECNRTL. As many units of the plant operate at high pressure and temperature where no liquid phase is present, the NRTL-RK model is applied. This model uses the Redlich–Kwong (RK) equation of state to describe the vapor phase and the non-random two-liquid model for the liquid phase (NRTL). For cooling water and steam, the STEAMNBS model is used since it counts with NBS/NRC equation of state for steam and liquid water properties (Haar et al., 1984).

Furthermore, Henry's law is applied to model the vapor–liquid equilibria for NO , NO_2 , O_2 , N_2 and N_2O_4 in the aqueous phase with Henry's law constants for NO_2 and N_2O_4 of $8.47 \cdot 10^6$ and $7.25 \cdot 10^4 \text{ m}^3\text{Pa}/\text{kmol}$ at 25 °C, respectively (Schwartz and White, 1981). It is assumed that Henry's law constants for NO_2 and N_2O_4 have a similar temperature dependency as that of SO_2 in water. The selected thermodynamic models for the sections in the nitric acid plant are summarized in Table 1.

Reaction kinetics

In the first step of the Ostwald process, ammonia is oxidized to form gaseous nitrogen oxides. Ammonia (NH_3) together with air passes over a Pt-Rh gauze catalyst composed of 90% platinum and 10% rhodium. The ammonia diffuses through the gaseous film to the catalyst surface, where it reacts with adsorbed oxygen to form nitric oxide (NO) and water (H_2O) (Eq. (1)) (Il'chenko, 1976). Eq. (1) to (3) thereby take place directly and are practically irreversible. All reactions are sufficiently exothermic to be self-sustaining. However, without the presence of a catalyst, mainly nitrogen would be formed. When a catalyst is used, Eq. (4) takes place only when the gas velocity is low and the formed nitrogen oxide diffuses into the catalyst. This secondary reaction can be avoided by decreasing the contact time between the catalytic wire gauze and the gases. For that reason, the gaseous mixture is quenched immediately to avoid NO decomposition (Koukolik and Marek, 1968). The catalytic combustion efficiency of ammonia is around 93 to 98



The Aspen Plus® operator used to simulate the catalytic oxidation unit is a stoichiometric reactor (R-101) considering a NH_3 conversion of 96% and 4% for Eqs. (1) and (3), respectively. The conversion of ammonia towards reactions (2) and (4) is quite low. Nowadays, catalysts for abatement are installed after the ammonia oxidation catalysts to reduce this greenhouse gas. Therefore, those reactions are neglected. A reduction of around 90% is feasible. Therefore, we neglected reactions (2) and (4) in our simulation. The catalytic combustion of ammonia proceeds as a combination of exothermic reactions at 890 °C. The released energy will be recovered by a series of heat exchangers. One of the main important economic and design aspects of this unit is the amount of catalyst required (Xin et al., 2017). A catalyst consumption of 0.11 g/ton nitric acid is taken from Sperner and Hohmann (1976). Assuming that the plant operates 8000 hours per year, a total of 25.7 kg of catalyst gauze is required for the process, of which around one-third must be replaced each year.

The second step of the Ostwald process is the oxidation of nitric oxide into nitrogen dioxide (NO_2) and dinitrogen tetroxide (N_2O_4). The remaining non-reacted oxygen from the ammonia combustion starts to react with the nitric oxide formed to produce NO_2 (Eq. (5)). This reaction occurs while the product gas of the ammonia combustion is cooled down, to recover the released heat Grande et al. (2018). At the same time, NO_2 can dimerize to form N_2O_4 (Eq. (6)). Consequently,

Table 1
Thermodynamic model for each section of the nitric acid plant.

Species	Section	Thermodynamic model
Air, Water and Ammonia	Air compression/Gas mixing	NRTL-RK
Air, steam and Ammonia	Ammonia oxidation	NRTL-RK
NO _x gases, Air and Ammonia	Nitric oxides oxidation	NRTL-RK
NO _x gases, Air, Water and Nitric acid	Absorption	ELECNRTL
Cooling water and Steam	Utilities	STEAMNBS

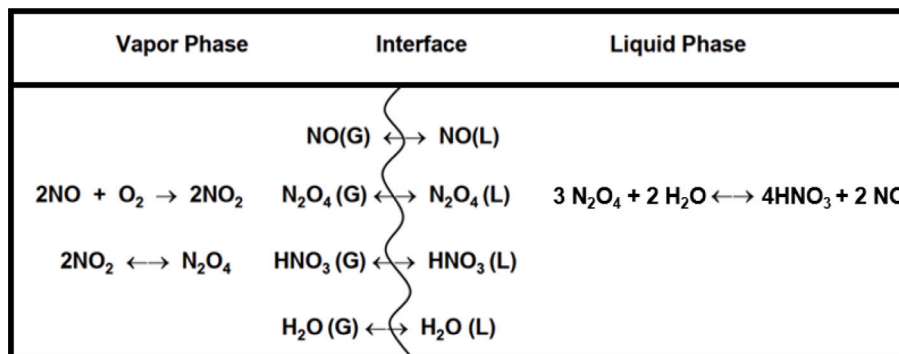
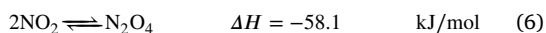


Fig. 3. Simplified absorption mechanism, developed by Miller (1987).

nitric oxide and NO₂ can react to form dinitrogen trioxide (N₂O₃) which is considered an undesirable reaction (Eq. (7)). The reaction of the NO_x gases with vaporized water leads to the formation of nitric acid (e.g. Eq. (8)).



The reactions (5), (6) and (8) are computed creating a Fortran user kinetic subroutine. The user subroutine is used to describe the kinetic model for several heat exchangers modeled as plug flow reactors (PFRs) in the nitric acid simulation. Other intermediate by-products such as nitrous acid (HNO₂) and N₂O₃ are unstable species and therefore not considered in the simulation. The specifications of the heat exchangers can be seen in the appendix Table A.5 and the applied reaction kinetics in Appendix A.1.

Finally, the last process step is the reactive absorption of NO₂ and N₂O₄ in water. NO_x absorption has been defined by many researchers as one of the most complex absorption mechanisms due to several reasons (Suchak and Joshi, 1994): Firstly, the obtained NO_x gas is a mixture of several nitrogen oxides (NO, NO₂, N₂O₃ and N₂O₄). The absorption of these NO_x gases in water leads to the formation of two oxyacids, nitric acid and nitrous acid. More than forty equilibrium reactions take place in both gas and liquid phase. The absorption of NO, NO₂, N₂O₃, and N₂O₄ is accompanied by chemical reaction whereas the desorption of NO, NO₂ and HNO₂ is preceded by chemical reaction. Secondly, there is a heterogeneous equilibrium between gas-phase and liquid-phase components and only limited or incomplete data of physical and chemical properties for the nitrogen oxides species are available.

Several methods have been proposed for calculating the complex absorption of nitrogen oxides in aqueous solution. They depend on the number of reactions considered, the factors included in the kinetic reactions and the different mathematical models used. We selected the simplified model developed by Miller in 1987, which uses correlations for modeling the behavior of absorption towers in the production of nitric acid (Miller, 1987). As Fig. 3 shows, this model considers two vapor-phase and one liquid-phase reaction. Firstly, the NO oxidation takes place to form NO₂ for which we assumed the kinetic rate

described by Bodenstein (1922). Secondly, the dimerization of NO₂ takes place. This equilibrium equation has been modeled using the equilibrium capability in Radfrac. Finally, the overall reaction for the production of nitric acid can be described. The absorption rate depends on the type of tray. In this work, sieve trays were chosen because they have become widely used in commercial nitric acid plants. The column specifications are shown in appendix Table A.6.

Oxygen injection in nitric acid plant

Several industry-approved patents are considering the injection of pure oxygen into nitric acid plants (Powell, 1975; Watson and Balke, 1980; Bhatia et al., 1997; Echegaray et al., 2000; Wagner and Plains, 2003). Based on these patents, four different injection cases are investigated to determine the feasibility and functionality of oxygen integration: **O₂ Bleacher**: Pure oxygen is uniquely injected in the upstream of the bleaching column, T-102; **O₂ Cooler**: Pure oxygen is uniquely injected in the upstream of the cooler/condenser, E-108; **O₂ Absorption**: Pure oxygen is uniquely injected in the upstream of the absorption tower, T-101; **O₂ Combustion**: Pure oxygen is uniquely injected into the primary feed air upstream the ammonia burner. An overview of the four different cases is given in Fig. 4.

The amount of surplus oxygen available from the hydrogen production is calculated according to the amount of ammonia needed to produce the 700 t/d of nitric acid. Theoretically, 3 moles of hydrogen and 1 mole of nitrogen are required to produce 2 moles of ammonia. Therefore, 0.177 t of hydrogen and 0.823 t of nitrogen are necessary to produce 1 ton of ammonia. Since 199.5 t/d of ammonia are needed to produce 700 t/d of nitric acid, 35.3 t/d of hydrogen are consumed. Applying Eq. (9), the surplus oxygen available from hydrogen production accounts for 131.3 t/d. Additionally, oxygen could be obtained from the air separation process for nitrogen production.



2.2. Explosion limits

The determination of the explosion limits for ammonia–oxygen–nitrogen mixtures for varying gas temperatures is based on a 0D-reactor network model in Cantera (Goodwin et al., 2022) (see Fig. 5). This model considers mass and species balances, an energy balance and applies the respective reaction mechanism. The CVODES solver integrates

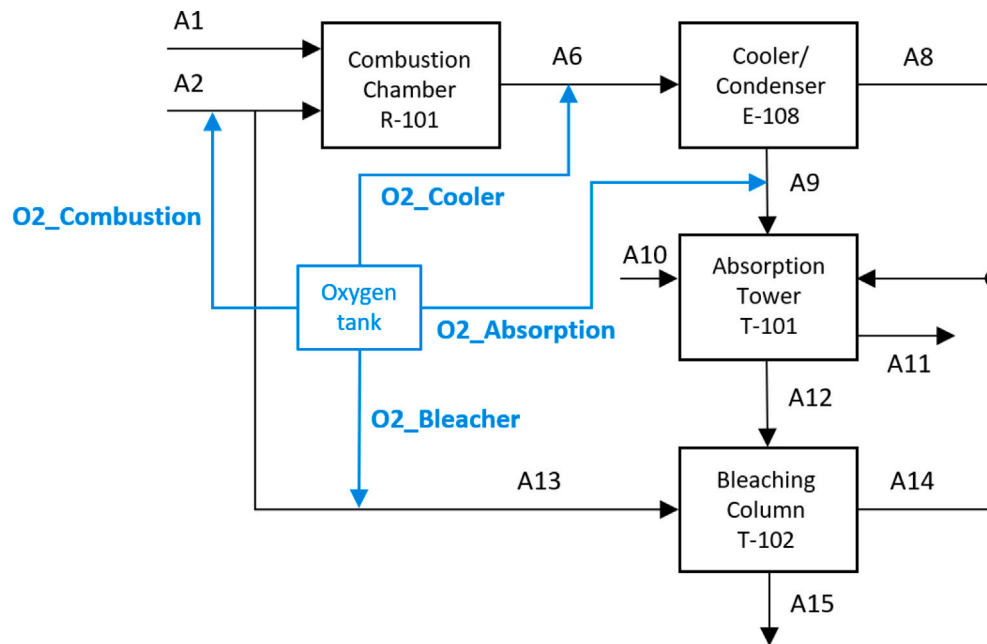


Fig. 4. Overview of injection cases of oxygen into the nitric plant. The flow names correspond to the flow diagram in 2.

the stiff ordinary differential equations for specified time steps to yield the time-dependant change in concentration, temperature and pressure in the reactor vessel. We implemented the reaction mechanism by Mei et al. (2019) as it gives satisfactory results for the laminar burning velocity of ammonia-air mixtures compared do experimental data (Mei et al., 2019; Liu and Han, 2021; Li et al., 2021).

The model is based on the following assumptions:

- The gases in the reservoir and reactor are homogeneously mixed.
- The reactor is adiabatic, has a constant volume and is in thermodynamic equilibrium.
- Explosion is detected when the gas temperature rises > 25 K/s in the reactor.

The defined reactor network consists of a fuel reservoir to provide the ammonia, an oxygen–nitrogen reservoir, an ignition source reservoir containing H atoms, a reactor for the combustion observation and an exhaust reservoir (see Fig. 5). The fuel and oxygen–nitrogen flows are mixed at predefined ratios and the total mass flow of the ammonia–oxygen–nitrogen mixture and the ignition source in the reactor is defined with mass flow controllers. These mass flows, the solver sensitivity and the reactor volume were varied in a sensitivity analysis to fit the results of this work’s model to literature values (Ciccarelli et al., 2006 for the lower explosion limits of ammonia-air mixtures from room temperature up to 400 °C at 1.013 bar. However, experimental literature values differ from each other, since the obtained explosion limit values depend on the experimental setup, the ignition source and the operating parameters. In our model a short gaussian-shaped pulse of H atoms from the ignition reservoir is applied to ignite the ammonia–oxygen–nitrogen mixture in the reactor. This initiated reaction in the reactor is simulated time-dependant and the temperature development of the reactor is tracked. The combustion in the reactor is considered as an explosion if the temperature in the reactor is increased by 50 K after 2 s run time (equal to 25 K/s), analogue to the numerical analysis of explosion limits for ammonia–hydrogen–oxygen mixtures from Liu and Han (2021). As no experimental or numerical data for explosion limits of oxygen-enriched air–ammonia mixtures could be found in literature, our results of this model were validated with experimental data for a nitrogen-diluted mixture for gas at room temperature, 300 °C and 400 °C (Harris and MacDermott, 1977). After this final step, the model was applied for an oxygen-enriched ammonia mixture at various

starting gas temperatures and pressures. The procedure and code for calculating the explosion limits are given in Appendix B.

2.3. Economic analysis

The methodology applied to develop the economic analysis is based on Peters, Timmerhaus and West (Peters et al., 2003). According to the level of detail provided, this study is estimated to be part of a class 3 & 4 following the ACE international guideline. These levels imply that the cost assessment accuracy is $\pm 30\%$ (Christensen et al., 2005). The calculations of the investment are based on the methodology for setting up a new system on an existing plant where the corresponding infrastructure is already in place.

The fixed capital investment (FCI) is the sum of direct and indirect equipment costs (EC). Eq. (10) is used to determine the equipment cost of each specific component, in which f_i represents the specific equipment cost function and $S_{i,k}$ corresponds to the equipment characteristic parameter which is needed to estimate the cost of the unit. $F_{pre,i}$ and $F_{mat,i}$ are additional equipment factors related to specific materials and operating conditions. The applied factors can be found in appendix Table D.8.

The Chemical Engineering Plant Cost Index (CEPCI) is a factor used to adjust process plant costs from one year to the selected base year, taking into account inflation and cost variations over time (Vatavuk et al., 2002; Maxwell, 2023). The techno-economic analysis in this work is performed for the year 2021. In appendix Table D.9 the values of the CEPCI and the \$/€ exchange rates from 2000 to 2021 are summarized. In addition, the equipment size is adapted applying Eq. (11). The fixed capital investment is estimated according to Eq. (12). The ratio factors ($F_{ind,i,j}$) for direct and indirect costs of fluid processing plants are given in the appendix (Table D.8). The total capital investment (TCI) is calculated assuming that 11% of the FCI is required as working capital (WC).

$$EC_{ref,i} = f_i(S_{i,1}; S_{i,2}; \dots; S_{i,k}) \cdot \frac{CEPCI}{CEPCI_{ref}} \cdot F_{pre,i} \cdot F_{mat,i}, \quad i, k \in N \quad (10)$$

$$EC_i = EC_{ref,i} \cdot \left(\frac{S_i}{S_{ref,i}} \right) \quad (11)$$

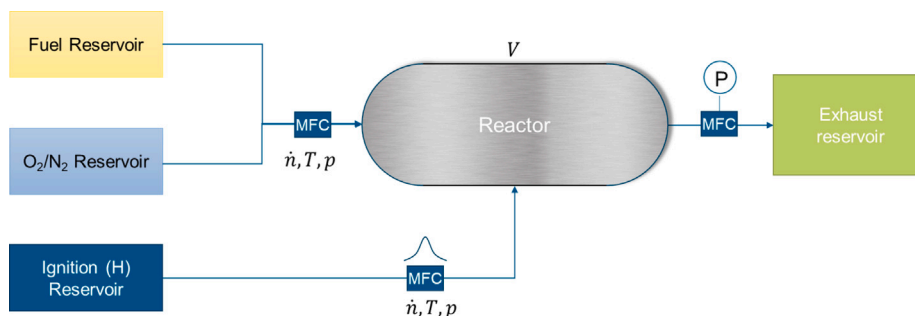


Fig. 5. Reactor network as defined with Cantera, for the analysis of explosion limits of ammonia–oxygen–nitrogen mixtures.

$$FCI = \sum_{i=1}^m \left(EC_i \cdot \left(1 + \sum_{j=1}^{12} F_{ind,i,j} \right) \right) \quad (12)$$

$$TCI = \frac{FCI}{0.89} \quad (13)$$

Operational expenses (OpEx) are divided into two categories: Direct OpEx and indirect OpEx (Eq. (14)). Direct operating costs are calculated based on the results of the process simulation and contain the costs of materials (\dot{m}) and utilities (P and Q). Indirect OpEx include e.g. maintenance, labor, supervision and administration costs. Estimations therefore are based on empirical data, taken from the chemical engineering design literature (Albrecht et al., 2017).

$$\sum OpEx_{direct} \left(\frac{\text{€}}{\text{year}} \right) = \sum_{i=1}^m \dot{m}_i \cdot c_{mat_i} + \sum_{j=1}^n P_j \cdot c_{power_j} + \sum_{k=1}^p Q_k \cdot c_{heat_k} \quad (14)$$

The Net Present Value (NPV) is the total amount of the present worth of all cash flows minus the present worth of all capital investments. The Minimum Selling Price of Product (MSP) is defined as the minimum product price that ensures a minimum investment target. It must be solved by iterating until the product price satisfies the equality constrain for NPV being zero for a given minimum acceptable rate of return (Peters et al., 2003).

The expected lifetime of the plant is assumed to be 15 years with a full load operating time of 8000 h per year. Depreciation is considered for the whole plant life time. The plant is assumed to be located in Spain, since Spain has the highest potential of solar energy in Europe (Gamarra et al., 2023). The cost references for raw materials and utilities are shown in Table 2. The economic analysis is performed based on the minimum selling price of nitric acid which meets an annual rate of return of 10%. The cash flow analysis is performed assuming a three years construction period in which 15%, 35% and 50% of the FCI is invested in the first, second and third year of the construction period respectively. The three years of the construction period are denoted as negative years in the cash flow analysis. Regarding the start-up cost, it is assumed a cost of 10% of FCI in the first year and two-year ramp up to reach full capacity with 50% production in the first year and 90% production in the second year. Spain has an income tax rate of 25% for large companies (PwC-Spain, 2023).

Three different types of nitric acid plants are considered in the economic evaluation. The reference plant is a conventional nitric acid plant (CON-NA), operated with fossil-based ammonia and electricity. The second nitric acid plant is fed with solar-based ammonia and electricity (SOL-NA). Therefore, hydrogen consumed in ammonia production comes from water electrolysis and the electric energy required in the Ostwald process is assumed to be obtained from a concentrated solar power plant. The last case is based on the optimized nitric acid plant (OXY-SOL-NA). It integrates the byproduct oxygen from the water electrolysis into the SOL-NA plant.

3. Results and discussion

3.1. Technical results

A special attention has been dedicated to simulate the complex NO_x absorption in aqueous solution (T-101). The columns stages are numbered from top to bottom (tray 1: top plate and tray 35: bottom plate). To obtain a nitric acid strength of 60 wt%, 236.5 t/d of process water is fed counter-current to the NO_x gases leaving the bleaching column and the condenser. Each stage of the absorption column is cooled with cooling water to maintain the temperature profile in favor of gas absorption.

The profile of the nitric acid mass composition in the absorption column is shown in Fig. 6(a). The strength of nitric acid increases in parallel with the acid production along the absorption tower. At the top of the column, the acid formation is almost negligible due to small contact time between NO_x gases and the process water. The closer it gets to the bottom of the column, the higher the liquid holdup. Therefore, the gas–liquid contact is superior leading to a higher acid production. Stage 28 of the absorption column is the optimum feed point for the acid stream from the cooler condenser (A9), since the acid composition in stream A9 is 42 wt% which corresponds to the concentration at this stage.

Controlling the NO_x emissions of a nitric acid plant is important, since NO_x emissions are strongly regulated. According to the Industrial Emissions Directive 2010/75/EU of the European Commission, NO_x emissions levels of nitric acid plants shall not exceed a NO_x concentration of 150 ppmv (Kamphus, 2014). Fig. 6(b) shows the profile of the nitric oxides gases along the absorption column. The concentration is exponentially decreasing from bottom to top as the gas stream is reacting and being absorbed by the liquid phase along the column. The remaining gases are leaving the column at a NO_x concentration of 623 ppmv. Further gas cleaning steps are required before exhaust gas can be released into the atmosphere. However, a DeNOx unit was not included in this study.

The four different oxygen injection cases are compared based on three metrics: the total acid production, the strength of the nitric acid and the NO_x concentration in the exhaust gas. Fig. 7(a) shows that oxygen injection can boost the nitric acid production up to 0.31% or 2.2 t/d. Comparing the different scenarios, increasing the oxygen content in the main air pipeline (A2) leads to the highest nitric acid production and strength (O2_Combustion). The second highest production is obtained for the case O2_Cooler, if oxygen injection occurs downstream the cooler condenser. Finally, O2_Bleacher and O2_Absorption show less promising results in terms of boosting the nitric acid production.

The nitric acid strength increases slightly as oxygen is injected (see Fig. 7(b)). Up to a maximum increase of 0.14 wt% can be obtained for the O2_Combustion case. Analogue to Fig. 7(a), it can be seen that there is a greater increase the earlier oxygen is injected into the process. Injecting oxygen upstream the ammonia burner will maximize the residence time of oxygen and will favor the conversion of NO to NO_2 . A

Table 2
Market prices for raw materials and utilities.

	Market price (2021)	Units	Reference
<i>Raw materials and utilities</i>			
Conventional ammonia	591.87	€/t	Elkin (2021)
Renewable ammonia (from electrolysis)	844.43	€/t	Campion et al. (2023)
Pt-Rh catalyst gauze	220.93	€/g	Aesar (2022)
Electricity from grid	128.00	€/MWh	Global petrol prices (2022)
Electricity CSP	136.67	€/MWh	Dersch et al. (2020)
Cooling water	0.05	€/m ³	Peters et al. (2003)
Process water	2.50	€/m ³	Selectra (2022)

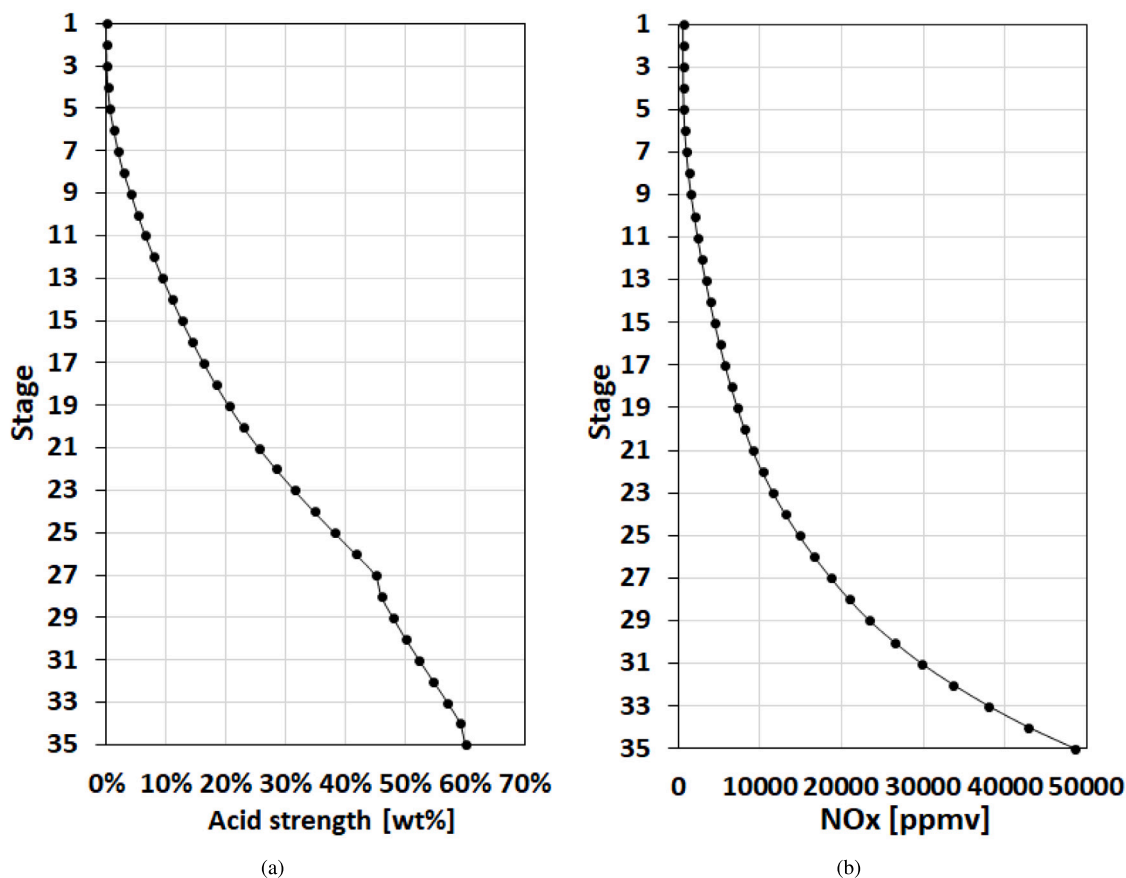


Fig. 6. Profiles along the absorption tower. (a) nitric acid strength (b) NO_x concentration in CONV-NA case.

higher amount of NO₂ will be available for the absorption with water, resulting in a greater production of nitric acid. Additionally, primary air and the bleaching air are compressed in the same compressor. Increasing oxygen content in the primary air stream (A2) reduces the load on the compressor and hence the power required. The power required for the compressors can be reduced by 7% by increasing the oxygen content in the primary air to 25.7 mol%. Likewise, the cooling heat duty during compression stages decreases as oxygen content is increased. Nevertheless, there are other factors that play a crucial role such as catalyst losses and the flammability of ammonia in air or oxygen enriched air, respectively. Increasing the residence time of oxygen in the burner will result in a higher catalyst loss due to rhodium and platinum react more frequently to form corresponding oxides (Echegaray et al., 2000). For safety reasons, the ammonia concentration must be low to avoid the lower explosion limit. The explosion limit also depends on the oxygen concentration, temperature, pressure, the flow velocity and the water content of the reaction mixture. The effect of increased oxygen concentration on the lower explosion limit is described in Section 3.2 to identify the upper oxygen injection limit for the O2_Combustion case.

Fig. 8 shows, how increasing the oxygen content in the conventional nitric acid plant will lead to a considerable decrease of the NO_x concentration in the tail-gas. A reduction of 28.66%, 32.96%, 29.56% and 43.6% for the NO_x concentration is achieved for the cases O2_Bleacher, O2_Cooler, O2_Absorption and O2_Combustion, respectively. Table 3 shows the summary of the maximum percentage increase for the injection cases evaluated. With a reduction of NO_x gas concentration of max. 44%, the exhaust gas cleaning unit could be drastically scaled down. The simulation of this unit is beyond the scope of this work, which explains why this reduction has not been addressed in economic and environmental terms. It can be expected that in case of a dual pressure plant, instead of a mono pressure plant as assumed for this work, the NO_x reduction could be further improved by oxygen injection. This is due to the higher pressure in the absorption tower compared to a mono pressure plant.

The trends in the results are in line with the patents discussed in Section 2.1. It can be concluded that injecting oxygen into nitric acid plants can boost the nitric acid production and the acid strength slightly, and moreover, significantly reduce the final NO_x gas concentration in the tail-gas.

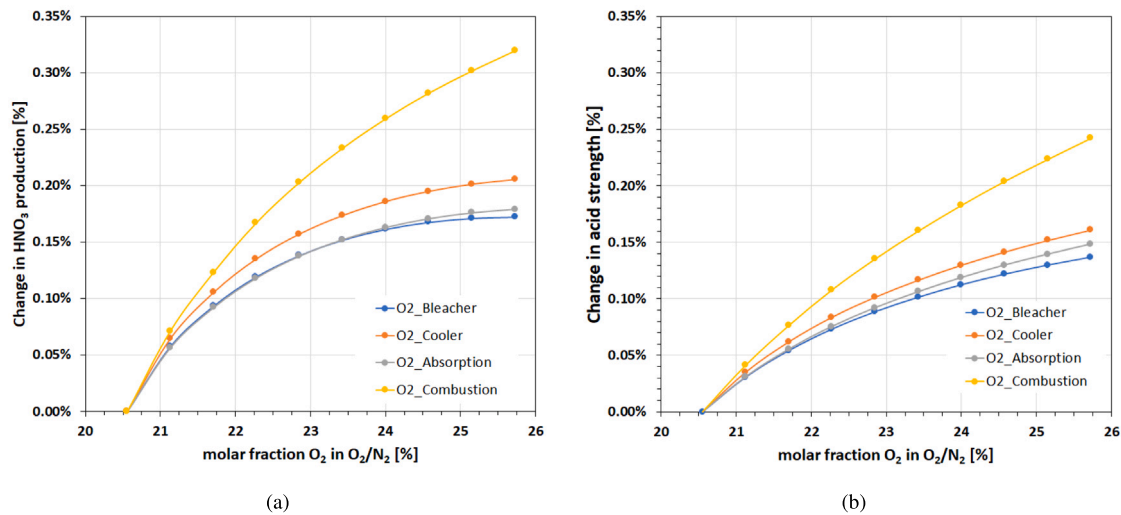


Fig. 7. Effect of oxygen injection on: (a) Nitric acid production (b) Nitric acid strength.

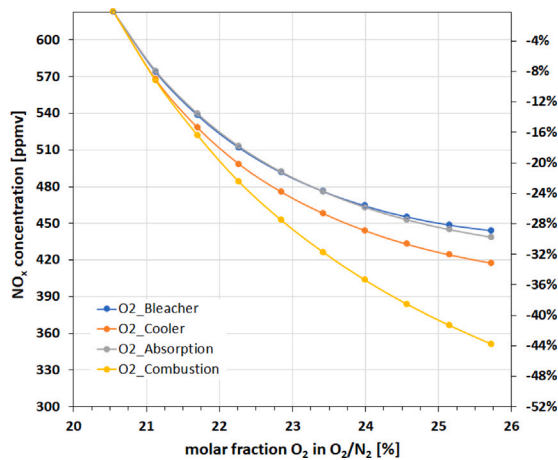


Fig. 8. Effect of oxygen injection on the absolute (left axis) and relative change (right axis) in NO_x concentration at the top of the absorption tower.

Table 3

Summary of the maximum improvement in acid production, acid strength or NO_x emissions for the four cases with 300 kmol/h oxygen injection.

Case	Acid production (%)	Acid strength (%)	NO_x concentration (%)
O2_Bleacher	0.17	0.14	-28.68
O2_Cooler	0.20	0.16	-32.96
O2_Absorption	0.17	0.15	-29.56
O2_Combustion	0.31	0.24	-43.60

3.2. Explosion limits

For safe operation of the nitric acid plant in the oxygen-injection case O2_Combustion, one must examine the effect of an increased oxygen concentration on the explosion limit of an ammonia–oxygen–nitrogen mixture in the ammonia burner. Therefore, we calculated the explosion limit for an oxygen-enriched atmosphere in the burner at corresponding pressures (1 to 5.8 bar) and gas inlet temperatures (up to 400 °C). An exemplary result for the time-dependant change of temperature, pressure, and O_2 and ammonia mole fraction of the OD simulation is given in the appendix (see Fig. B.15). These plots demonstrate the difference in the temperature and pressure change around the lower explosion limit (LEL) at 20 °C and 1.013 bar in comparison to the pure combustion of the ignition source. In this example, only ammonia

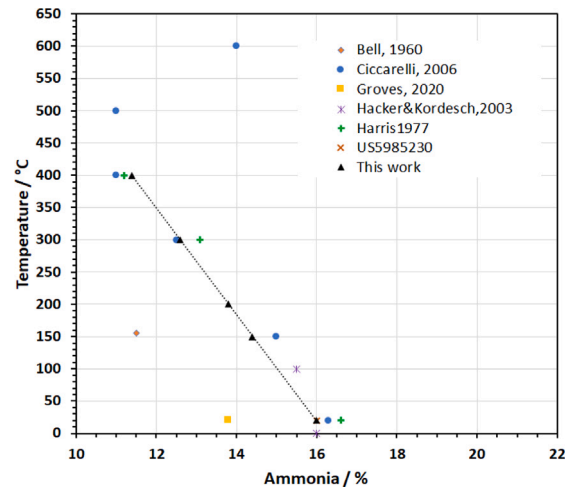


Fig. 9. Comparison of literature values (Bell, 1960; Ciccarelli et al., 2006; Groves, 2000; Hacker and Kordesch, 2003; Harris and MacDermott, 1977; Powell, 1975) and own results for the lower explosion limit of ammonia-air mixtures at various temperatures.

concentrations above 15.9% result in a combustion after the burning of the ignition source.

The code was validated with experimental data from literature for ammonia-air mixtures (see Fig. 9) up to 400 °C. The compression of the air previous to the ammonia burner leads to max. 400 °C for 10 bar operation, or 300 °C for a 7 bar operation (Haynes, 2019). A satisfactory deviation between the experimental data from Ciccarelli et al. (2006) and our results of maximum $\pm 4\%$ was observed.

The effect of enriching or diluting ammonia-air mixtures on the lower and upper explosion limit (UEL) at various temperatures is displayed in Fig. 10(a). For diluted air–ammonia mixtures experimental data from Harris and MacDermott (1977) is available and can be used for comparison. Our simulation results yield a similar trend of an increased explosion area at higher temperatures and a maximum deviation from the experimental LEL values of nitrogen-enriched ammonia mixtures of $\pm 14\%$. In general, the change in oxygen concentration is drastically influencing the upper explosion limit, whereas it shows only a minor impact on the lower explosion limit, i.e. from 21% to 30% oxygen the LEL decreases only from 16% to 15.9% ammonia at 20 °C. As expected, a higher gas inlet temperature decreases the LEL,

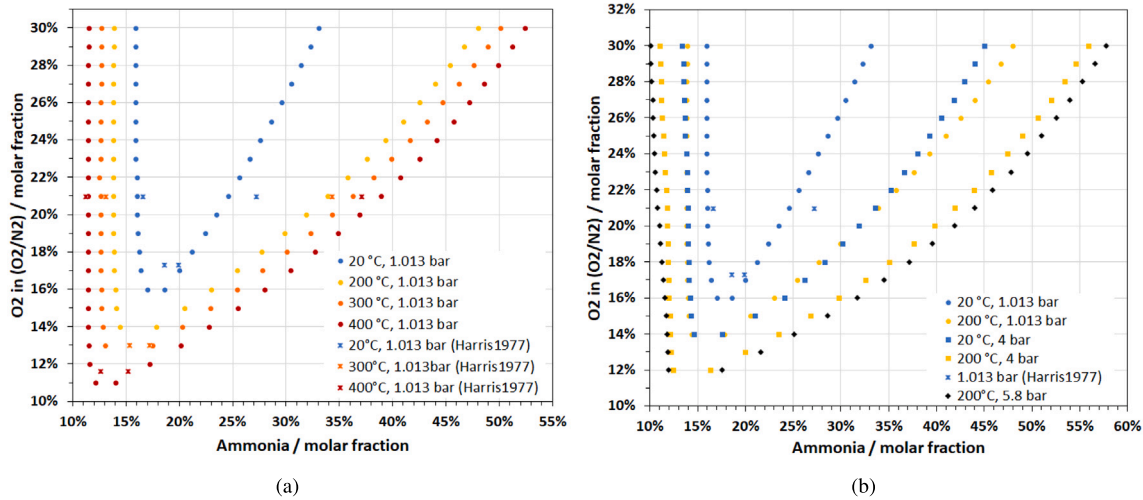


Fig. 10. Comparison of literature values (Harris and MacDermott, 1977) and own results for the explosion limits of ammonia-O₂-N₂ mixtures at a) atmospheric pressure and 20 °C, 200 °C, 300 °C and 400 °C and b) atmospheric pressure or 4 bar.

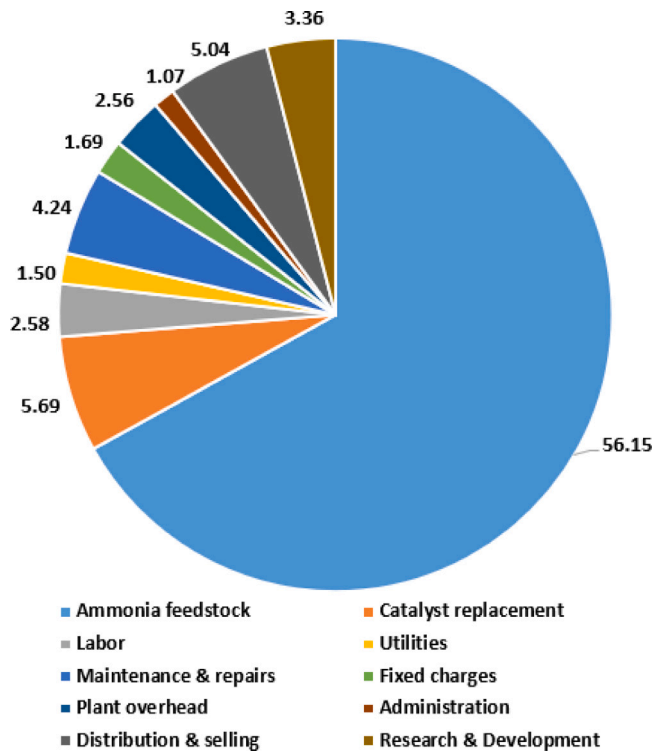


Fig. 11. OpEX distribution of the OXY-SOL-NA plant in M€/a, excluding capital cost.

i.e. to 11.4% at 400 °C. The increase of pressure also reduces the lower explosion limits (see Fig. 10(b), i.e. from 13.8% (21% O₂, 200 °C, 1.013 bar) to 11.8% (21% O₂, 200 °C, 4 bar).

The nitric acid plant under the O₂Combustion operation mode uses an oxygen molar fraction of max. 25.7% in the oxygen–nitrogen mixture and a total ammonia molar fraction of 9.9%. This is still below the calculated LEL for gas inlet temperatures of 20 °C and atmospheric pressure of 16%. However, operating the ammonia burner at elevated pressures reduces the capital cost of the burner and can yield higher NO concentrations (Haynes, 2019). Thus, in our study we assumed gas inlet conditions of 200 °C and 5.8 bar, which results in a LEL of 10.3% ammonia with oxygen-enriched air (26% molar fraction of O₂ in O₂/N₂-mixture) or a LEL of 10.8% in air. Therefore, the used

Table 4

Economic results for the investigated nitric acid plants.

Type of plant		CON-NA	SOL-NA	OXY-SOL-NA
FCI	M€	85.06	85.06	84.61
WC	M€	10.51	10.51	10.46
TCI	M€	95.58	95.58	95.07
Direct OpEx	M€/y	53.39	70.21	70.16
Indirect OpEx	M€/y	11.92	13.81	13.78
Total OpEx	M€/y	65.31	84.02	83.94
Plant capacity	kt/y	388.9	388.9	390.1
MSEP	€/t	220.0	268.4	267.1

molar ammonia fraction in the process simulation is also for the highest oxygen injection case still below the LEL. The steam content in the combustion gases of the process simulation would further increase the LEL, as the LEL calculation only considered dry gases. Nevertheless, these calculations should be only considered as an indication and could be used to prepare explosion limits experiments for higher oxygen concentrations.

3.3. Economic results

In Section 2.3 three different economic scenarios were defined which are examined with regard to capital costs, operating costs and minimum selling price of the product. The conventional nitric acid plant CON-NA leads to the lowest MSP of 220 \$/t for nitric acid with a purity of 60% in water. The solar based plant SOL-NA powered with electricity from a CSP plant and utilizing renewable ammonia has a MSP of 268 \$/t. For the technical optimized OXY-SOL-NA plant where surplus oxygen is injected into the primary air (case O₂Combustion), the solar nitric acid costs can be reduced to 267 \$/t. According to ChemAnalyst the nitric acid price varied from 2021 to 2023 between 196 \$/t and 280 \$/t (60%wt) in Europe or North America, which is in line with the calculated results (ChemAnalyst, 2023). The comparison of the economic results of the three different plants is presented in Table 4. The full capital investment of the three plants is almost the same, since the size and costs of the needed equipment differ only slightly. A small variation in the OXY-SOL-NA plant can be explained with the smaller compressor needed to compress the feed air stream (see appendix Table D.11).

Nevertheless, the operational expenses of the CON-NA plant are 22% lower compared to SOL-NA and OXY-SOL-NA plants. This can

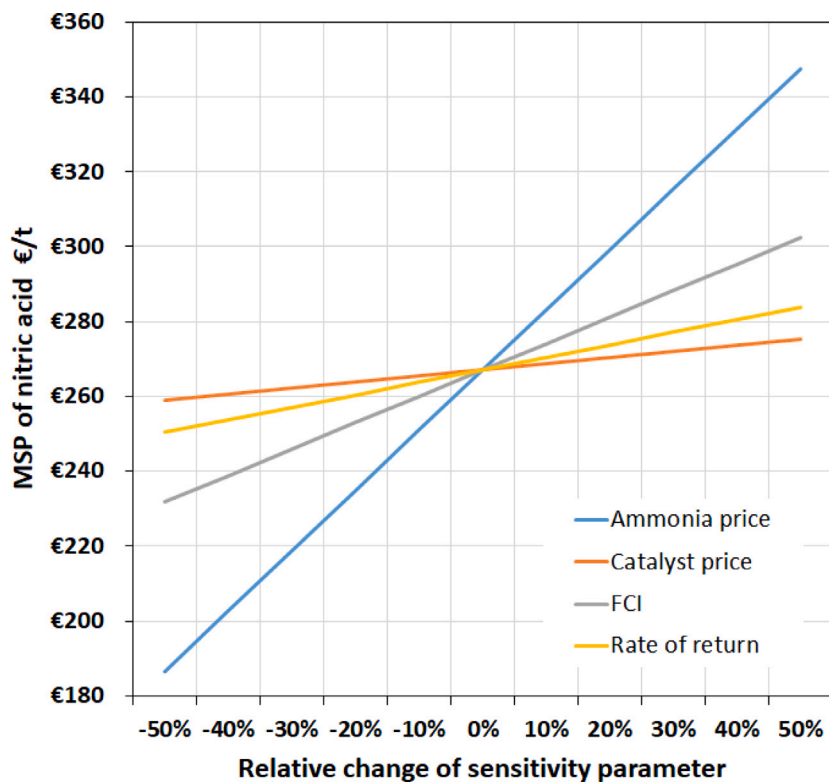


Fig. 12. Sensitivity analysis of the main cost drivers for the OXY-SOL-NA plant.

mainly be explained by the ammonia price which is the main cost driver of the operating costs of the nitric acid plants. In fact, the assumed cost of solar ammonia is 43% higher than the conventional ammonia (see Table 2). And the costs of ammonia constitute 60% of the total OpEx of the CON-NA plant and 67% of the solar based plants (see Fig. 11). However, cost assumptions for the ammonia market price are critical to define, since the ammonia cost varied from 200 to 900 \$/t between 2008 and 2021 (Elkin, 2021). The same applies to the cost of renewable ammonia, since it is not produced in high capacities yet and data are based on techno-economic assessments which are associated with uncertainties (Campion et al., 2023; Budinis et al., 2021; Lee et al., 2022).

In addition to the above described scenarios, the effect of CO₂-certificate pricing onto the cost of conventional nitric acid production and especially conventional ammonia is evaluated. Ammonia production can be related to 2.5 tons of CO₂ per ton of ammonia (Wernet et al., 2016). Assuming that 57% of the emissions have to be auctioned in phase 4 of the ETS (European Parliament and Council, 2023), the price of the CO₂-certificates has to increase by 173 €/t_{CO₂} to reach the break even point where the conventional nitric acid has the same MSP as the solar nitric acid for the optimized plant. In Q4 of 2021 the certificate price was around 60 €/t_{CO₂} (Trading Economics, 2023) which would lead to a total of 233 €/t_{CO₂}. Therefore, CO₂ pricing policies could make the implementation of green ammonia in the nitric acid plant feasible in future.

The influence of the NO_x concentration in the exhaust gas and the gas cleaning on the final product cost has not been evaluated, but could have an influence on the final product cost for the different scenarios. Especially regarding the significant reduction of NO_x emissions for the OXY-SOL-NA case.

3.3.1. Sensitivity analysis

Based on the most dominant cost contributions to the operational expenses shown in Fig. 11 a sensitivity analysis is performed to evaluate

the influence of different assumptions on the final nitric acid price. The sensitivity analysis has been performed for all three plant types. However, as all plant types show the same effect the discussion focuses on the OXY-SOL-NA plant as an example (see Fig. 12). In addition to the most dominant OpEx contributions, FC and ROI is also varied. FCI is predicted to be accurate from -30% to +30% (see Section 2.3), resulting in an MSP between 246 and 288 \$/t_{HNO₃} or +/- 8%. The purchase costs of ammonia and the catalyst is varied within a range of -50% to +50% in order to observe the impact on the MSP of nitric acid. Additionally, the full capital investment and the rate of return have also been varied in between this range. It can be noticed that the ammonia cost is the most sensitive parameter for the MSP of nitric acid. The price of nitric acid could be reduced by up to 30% if the cost of ammonia were reduced by 50%.

Currently, green ammonia is mainly dependent on the price of green hydrogen production. CO₂ pricing policies could make the implementation of green ammonia in the nitric acid production process feasible in the near future.

4. Conclusion

In this study, we have evaluated the effect of injecting surplus oxygen from ammonia production in the subsequent Ostwald process with a techno-economic assessment for a mono-pressure plant with a capacity of 700 t/d. In general, the injection of surplus oxygen from the renewable ammonia production into the Ostwald process leads to a better performance of the nitric acid production compared to the conventional process in all investigated cases. Especially the NO_x reduction in the exhaust gas of the absorption column shows the potential to run the fertilizer production more economical with a downscaled DeNO_x unit. The best efficiency of the process could be achieved if oxygen is injected directly into the primary air upstream of the ammonia combustion (O₂ combustion). For this case, an increase in nitric acid production of 0.31%, a higher acid strength of 0.24%,

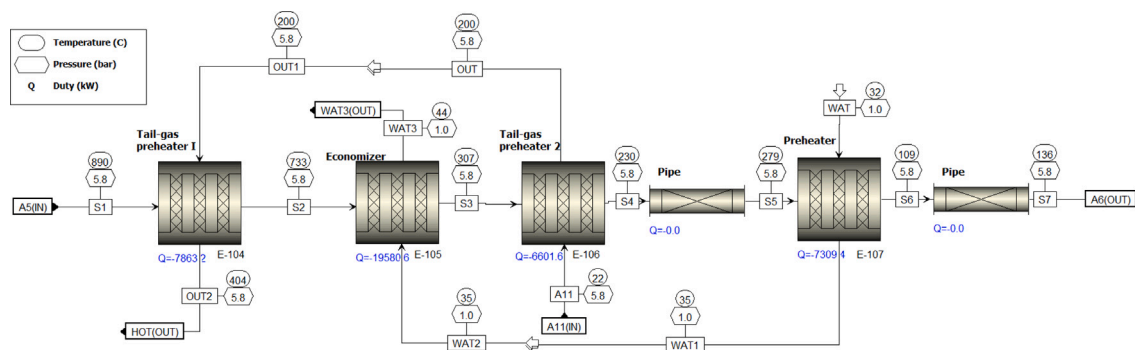


Fig. A.13. Heat-recovery unit: series of heat exchangers.

Table A.5
Reactive heat exchangers specifications.

Identification code	E-104	E-105	E-106	E-107	E-108
Operating parameters	Values				
Reactor type	RPlug (Reactor with counter-current thermal fluid)				
Reaction set	Model 2				
Heat transfer coefficient (W/m ² K)	1280	204	189	233	1220
Thermal fluid outlet temperature (°C)	404	44	200	35	32
Number of tubes	–	643	1527	1527	1200
Length of tubes (m)	3.2	4.2	3.0	3.0	5.6
Diameter of tubes (m)	1.220	0.025	0.015	0.015	0.014

and a decrease in NO_x concentration in the exhaust gas of 44% are observed. In future, the effect of oxygen injection on N₂O reaction and its catalytic abatement should be considered as well.

Furthermore, the investigation of the explosion limits of an nitrogen–oxygen–ammonia gas mixture was carried out via 0D-reactor modeling. The simulated values largely correlate with experimental values from the literature. The modeling leads to the conclusion that under the given process conditions security issues may arise. For 200 °C and 5.8 bar of the feed-gas before the ammonia burner, there is a low safety margin to the lower explosion limit of 10.3% for dry mixtures. Further simulative and experimental investigations of the lower explosion limit of the ammonia–air mixture must be carried out, also considering a steam content in the gas mixture. A possible option to adapt the process for a higher safety margin would be to inject surplus oxygen directly into the ammonia burner, or to reduce the pressure of the ammonia/oxygen/nitrogen mixture. Alternatively, injecting oxygen in the cooler presents the second best improvement with a NO_x concentration reduction of –33%.

Finally, the economic assessment shows that the final product price of nitric acid strongly correlates with the purchased ammonia. Therefore, the conventional process (CON-NA) has the lowest production cost of 220 \$/t of nitric acid (60 wt% in water) which is 22% lower than the solar produced nitric acid (SOL-NA) of 268 \$/t. The technical optimized process which includes oxygen injections (OXY-SOL-NA), the nitric acid price can be slightly reduced to 267 \$/t. This can be explained by the lower investment and energy demand for the feed-gas compressor and also the increase in capacity. Taking into account CO₂-certificates, a break-even point of the CON-NA and the OXY-SOL-NA could be reached for a certificate price of 233 €/t_{CO₂}. The benefits of a cleaner exhaust gas with a lower NO_x concentration for the OXY-SOL-NA plant is not considered in the economic evaluation, but could push the balance in the direction of the renewable process.

CRedit authorship contribution statement

Nicole Carina Neumann: Conceptualization, Formal analysis, Investigation, Methodology, Project administration, Software, Supervision, Validation, Visualization, Writing – original draft, Writing – review & editing. **David Baumstark:** Conceptualization, Data curation,

Formal analysis, Investigation, Methodology, Supervision, Validation, Visualization, Writing – original draft, Writing – review & editing. **Pablo López Martínez:** Data curation, Formal analysis, Investigation, Methodology, Software, Validation, Visualization, Writing – original draft, Writing – review & editing. **Nathalie Monnerie:** Funding acquisition, Resources. **Martin Roeb:** Funding acquisition, Project administration, Resources, Writing – original draft.

Declaration of competing interest

The authors declare that they have no known competing financial interests or personal relationships that could have appeared to influence the work reported in this paper.

Data availability

Data will be made available on request.

Acknowledgments

This work has received funding from project SESAM (EFRE-0801-808), which is co-funded by the federal state of North Rhine-Westphalia, Germany. The authors wish to thank Dr. Johannes Dammeier from Thyssenkrupp for his feedback regarding the modeling results and the fruitful discussions.

Appendix A. Technical specifications

A.1. Oxidation of nitrogen oxides in reactive heat exchangers

The heat released from the multiple exothermic reactions (Eqs. (1) to (4)) is recovered in a series of heat exchangers called heat-recovery unit (Fig. A.13). A hierarchy block has been used to simulate the heat recovery unit. This unit is composed of four reactive heat exchangers modeled as plug flow reactors and two pipes modeled as adiabatic reactors. Fig. A.13 shows, how the heat released from the catalytic combustion of ammonia (A5 at 890 °C) is recovered by the heat-exchanger train (A6 at 136 °C). The thermal energy of the tail-gas

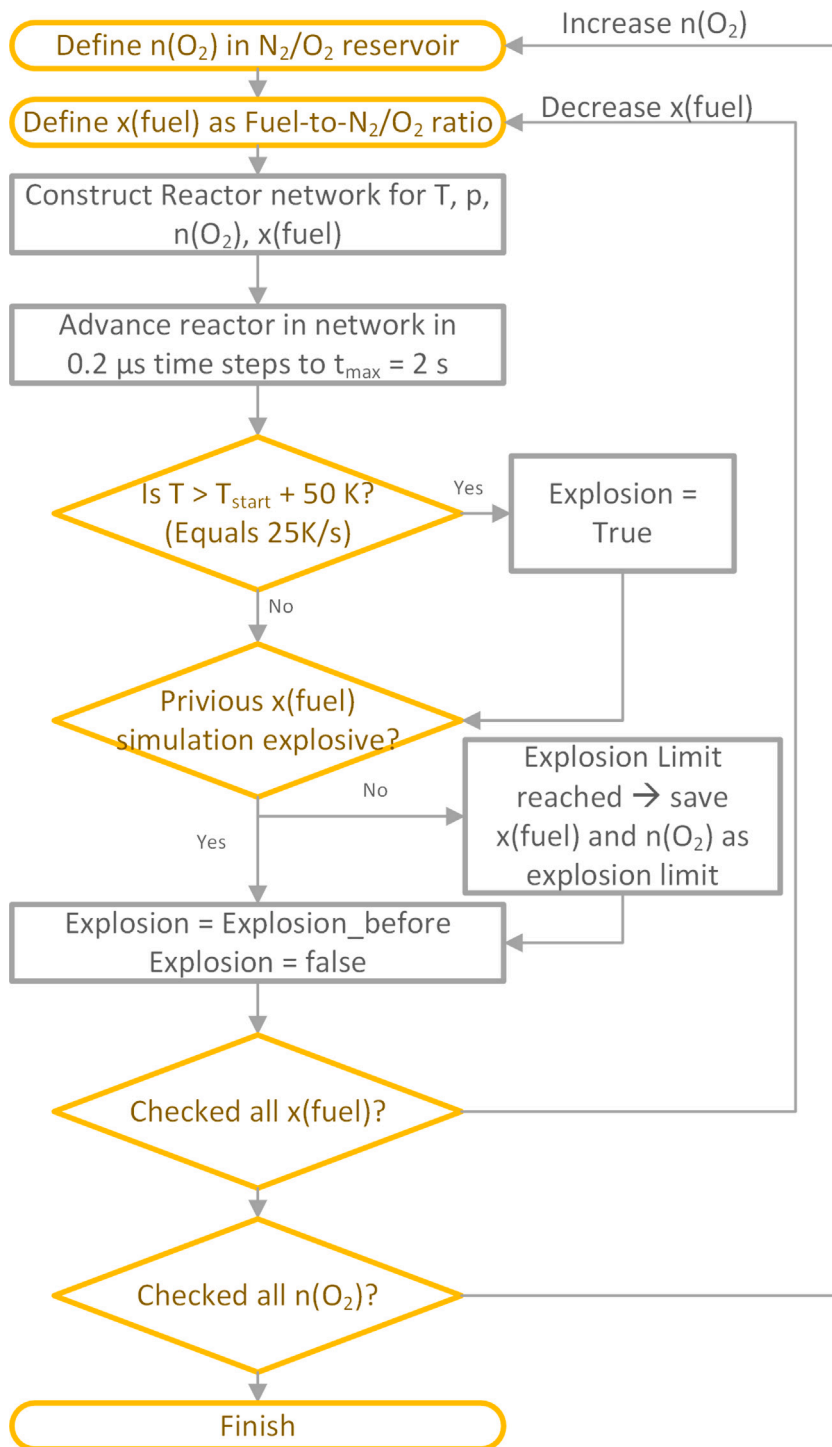


Fig. B.14. Applied algorithm to obtain explosion limits for ammonia-air-nitrogen mixtures.

Table A.6
Absorption and bleacher column specifications.

Identification code	T-101	T-102
Operating parameters	Value	Value
Column type	RadFrac	RadFrac
Reaction set	Model 3	Model 3
Calculation type	Equilibrium	Equilibrium
Condenser	Partial	None
Reboiler	None	None
Convergence mode	Strongly non-ideal liquid	Strongly non-ideal liquid
Number of plates	35 (Sieve trays)	8 (Sieve trays)
Column diameter (m)	5.5	3.37
Holes diameter (m)	0.1	0.1
Pressure (bar)	5.8	5.8
Feed streams	A9 (plate 28), A10 (plate 1) & A14+A15 (plate 35)	A12 (plate 1) & A13 (plate 1)
Outlet streams	A11 (plate 1) & A12 (plate 35)	A14 (plate 1) & A15 (plate 8)
Bottom temperature (°C)	55	Not defined
Top temperature (°C)	22	Not defined

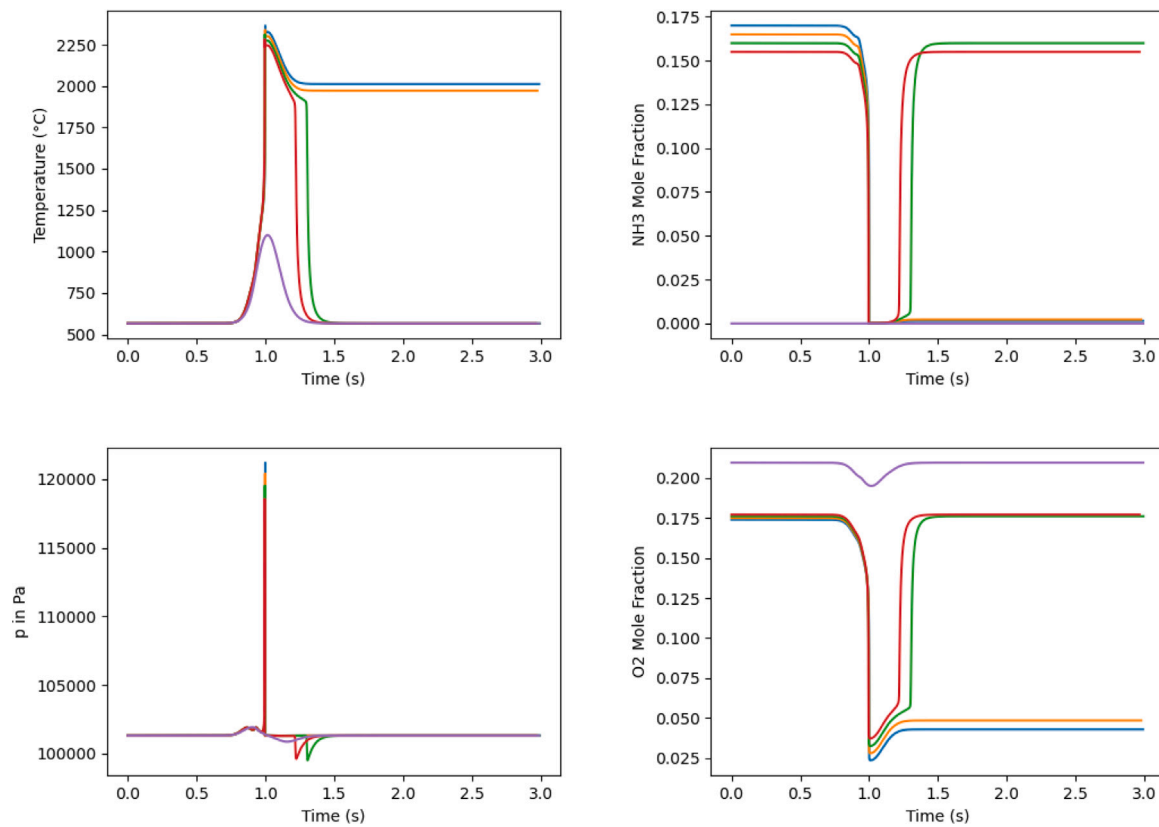


Fig. B.15. Change of temperature, pressure, NH_3 mole fraction and O_2 mole fraction for 5 different $\text{NH}_3\text{-O}_2\text{-N}_2$ mixtures at 20 °C and 1.013 bar.

leaving the absorption column (A11) is used in the units E-104 and E-106. On the other hand, cooling water is needed for the units E-105, E-107 and E-108. The specifications of the heat exchangers are summarized in Table A.5.

The oxidation of nitric oxide to nitrogen dioxide is a slow homogeneous reaction which is favorable at low temperatures and high pressures. At temperatures below 150 °C and with sufficient residence time, almost all of the nitric oxide is converted to nitrogen dioxide. The reverse reaction of Eq. (5) gains importance at low temperatures. Therefore, the forward and backward reaction rates need to be considered (Rate (A.1) & (A.2)) (Bodenstein, 1922).

$$r_{3.2f} = \frac{k_{3.2f}}{RT} P_{\text{NO}}^2 P_{\text{O}_2}; \quad \log k_{3.2f} = (-1.0366 + \frac{652.1}{T}) \text{ atm}^{-2} \text{ s}^{-1} \quad (\text{A.1})$$

$$r_{3.2b} = \frac{k_{3.2b}}{RT} P_{\text{NO}_2}^2; \quad k_{3.2b} = \frac{k_{3.2f}}{K_{eq}}; \quad \ln K_{eq} = (-17.9956 + \frac{13870.9}{T}) \text{ atm}^{-1} \quad (\text{A.2})$$

The second equilibrium reaction (Eq. (6)) corresponds to the dimerization of nitrogen dioxide. This reaction reaches rapidly the equilibrium state. As Le Chatelier's principle indicates, lower temperature and high pressure shift the equilibrium towards the production of dinitrogen tetroxide. Nevertheless, during the whole heat recovery unit only a small fraction of nitrogen dioxide is converted into dinitrogen tetroxide.

$$r_{3.3f} = \frac{k_{3.3f}}{RT} P_{\text{NO}}^2; \quad k_{3.3f} = 10 \cdot k_{3.2f} \text{ atm}^{-1} \text{ s}^{-1} \quad (\text{A.3})$$

Table C.7
Summary of industry-approved patents.

Injection location	Upstream combustion chamber	Upstream cooler/Condenser	Upstream absorption column	Upstream bleaching column
US3927182A ^a (Powell, 1975)	NC	NC	NC	NC
US4183906 (Watson and Balkey, 1980)	NC	NC	C	C
CA2200996A1 (Bhatia et al., 1997)	NC	NC	C	NC
US6165435A (Echegarary et al., 2000)	C	C	C	C
EP0808797A3 (Wagner and Plains, 2003)	NC	C	NC	C

^a = only tail gas recovery considered

C = Considered

NC = Not considered

Table D.8
Direct and indirect cost factors of a fluid processing plant (Peters et al., 2003; Albrecht et al., 2017).

Indirect cost items, $F_{ind,i,j}$	j	Basis	Typical value
<i>Total direct plant costs (D)</i>			
Equipment installation	1	EC	0.47
Instrumentation and control	2	EC	0.36
Electrical systems (installed)	3	EC	0.68
Piping (installed)	4	EC	0.11
Buildings (including services)	5	EC	0.18
Yard improvements	6	EC	0.1
Service facilities (installed)	7	EC	0.55
<i>Total indirect plant costs (I)</i>			
Engineering and supervision	8	EC	0.33
Construction expenses	9	EC	0.41
Legal expenses	10	EC	0.04
Contractor's fee	11	EC	0.2
Contingency	12	EC	0.4

Table D.9
\$/€ exchange rate and CEPCI from 2000 to 2021 (European Central Bank, 2023; Maxwell, 2023).

Year	\$/€	CEPCI
2000	0.924	394.1
2001	0.896	394.3
2002	0.946	395.6
2003	1.131	402.0
2004	1.244	444.2
2005	1.244	468.2
2006	1.256	499.6
2007	1.371	525.4
2008	1.471	575.4
2009	1.395	521.9
2010	1.326	550.9
2011	1.392	585.7
2012	1.285	584.6
2013	1.328	567.6
2014	1.329	576.1
2015	1.110	557.0
2016	1.107	542.0
2017	1.130	567.5
2018	1.181	600.0
2019	1.120	607.5
2020	1.142	599.5
2021	1.183	708.8

$$r_{3,3b} = \frac{k_{3,2b}}{RT} P_{N_2O_4}; \quad k_{3,3b} = \frac{10 \cdot k_{3,2f}}{K_{eq}}; \quad \ln K_{eq} = (-21.244 + \frac{6891.6}{T}) \text{ atm}^{-1} \quad (\text{A.4})$$

A rate constant of 10 times the NO oxidation reaction has been used for the forward reaction. This factor can be considered as an adjustable parameter in controlling the reaction rate for nitrogen dioxide dimerization (Aspen Technology, Inc., 2004).

Table D.10
Indirect OpEx by Albrecht et al. (2017).

Investment item	j	Basis	Typical factor
Operating supervision	1	Operating labor (OL)	0.15
Maintenance labor	2	FCI	0.01–0.03
Maintenance material	3	FCI	0.01–0.03
Operating supplies	4	Total maintenance costs	0.15
Laboratory charges	5	OL	0.2
Insurance and taxes	6	FCI	0.02
Plant overhead costs (PO)	7	Total labor costs	0.6
Administrative costs	8	PO	0.25
Distribution and selling costs	9	Net present cost	0.06
Research and development costs	10	Net present cost	0.04

Finally, the last reaction is the formation of nitric acid from water and nitrogen dioxide (Eq. (8)). This reaction takes place really fast in gas-phase until it reaches equilibrium. The equilibrium constant used for this reaction comes from the Koukolik and Marek investigation (Koukolik and Marek, 1968).

$$r_{3,4f} = \frac{k_{3,4f}}{RT} P_{NO_2}^3 P_{H_2O}; \quad k_{3,4f} = 8000 \cdot k_{3,2f} \text{ atm}^{-3} \text{ s}^{-1} \quad (\text{A.5})$$

$$r_{3,4b} = \frac{k_{3,4b}}{RT} P_{HNO_3}^2 P_{NO}; \quad k_{3,4b} = \frac{k_{3,4f}}{K_{eq}}; \quad \ln K_{eq} = (-19.7292 + \frac{4282.34}{T}) \text{ atm}^{-1} \quad (\text{A.6})$$

The reaction rate constant for the forward reaction has been set to 8000 the basic NO oxidation rate constant. This factor is chosen to simulate effectively the equilibrium model (Aspen Technology, Inc., 2004).

A.2. Column specifications

The specifications of the absorption and the bleaching column are summarized in Table A.6.

Appendix B. Explosion limits

The algorithm for the explosion limit determination is displayed in Fig. B.14. The code for the explosion limits calculations can be found in the supplementary data.

Appendix C. Patents regarding optimized nitric acid plants

In Table C.7 patents are summarized which include the oxygen injection into the nitric acid production.

Appendix D. Economic parameters

See Table D.10.

Table D.11
Equipment costs of the investigated nitric acid plant configurations.

Equipment	Code	$S_{ref} 1^a$	Unit	EC ^a M€ ₂₀₂₁	EC ^b M€ ₂₀₂₁	Source
Ammonia evaporator	E-101	2.03	m ² (exchange area)	0.005	0.005	Peters et al. (2003)
Ammonia preheater	E-102	3.38	m ² (exchange area)	0.005	0.006	Peters et al. (2003)
Ammonia–air preheater	E-103	28.44	m ² (exchange area)	0.011	0.012	Peters et al. (2003)
Tail-gas preheater I	E-104	12.07	m ² (exchange area)	0.007	0.008	Peters et al. (2003)
Economizer	E-105	212.10	m ² (exchange area)	0.049	0.053	Peters et al. (2003)
Tail-gas preheater II	E-106	215.87	m ² (exchange area)	0.049	0.053	Peters et al. (2003)
Feedwater preheater	E-107	215.87	m ² (exchange area)	0.049	0.053	Peters et al. (2003)
Cooler-Condenser	E-108	295.00	m ² (exchange area)	0.064	0.069	Peters et al. (2003)
Bleacher preheater	E-109	17.49	m ² (exchange area)	0.009	0.009	Peters et al. (2003)
Air compressor	C-101	10.23	MW (electric power)	9.967	9.862	Peters et al. (2003)
Combustion Chamber	R-101	12.50	m ³ (reactor volume)	0.139	0.139	Rehman et al. (2007)
Absorption Column	T-101	1021.14	m ³ (column volume)	5.400	5.398	Peters et al. (2003)
Bleaching Column	T-102	178.48	m ³ (column volume)	1.013	1.012	Peters et al. (2003)
Feedwater pump	P-101	3.20	kW (electric power)	0.006	0.006	Peters et al. (2003)
Total:				16.77	16.68	

^a CON-NA & SOL-NA

^b OXY-SOL-NA

Appendix E. Supplementary data

Supplementary material related to this article can be found online at <https://doi.org/10.1016/j.jclepro.2024.140740>.

References

- Aesar, A., 2022. Platinum rhodium gauze, 80 mesh woven from 0.076mm. URL <https://www.alfa.com/en/catalog/012217/>.
- Albrecht, F.G., König, D.H., Baucks, N., Dietrich, R.-U., 2017. A standardized methodology for the techno-economic evaluation of alternative fuels – a case study. *Fuel* 194, 511–526. <http://dx.doi.org/10.1016/j.fuel.2016.12.003>, URL <https://www.sciencedirect.com/science/article/pii/S0016236116312248>.
- Aspen Technology, Inc., 2004. Nitric Acid package. Technical Report.
- Bell, B., 1960. Platinum catalysts in ammonia oxidation. *Platinum Met. Rev.* 4 (4), 122–126, URL <https://www.ingentaconnect.com/content/matthey/pmr/1960/00000004/00000004/art00001>.
- Bhatia, S., Jacko, F., Vlaming, R., König, J., 1997. Oxygen injection in nitric acid production. Canadian Patent 2200996A1.
- Bodenstein, M., 1922. Bildung und Zersetzung der höheren Stickoxyde. *Zeitschrift für Physikalische Chemie* 100 (1), 68–123.
- Budama, V., Duarte, J.P.R., Roeb, M., Sattler, C., 2022. Potential of solar thermochemical water-splitting cycles: A review. *Sol. Energy* 249, 353–366, URL <https://elib.dlr.de/192060/>.
- Budinis, S., Gouy, A., Levi, P., Mandová, H., Vass, T., 2021. Ammonia Technology Roadmap. Towards more sustainable nitrogen fertiliser production. Technical Report, International Energy Agency, pp. 1–168.
- Campion, N., Nami, H., Swisher, P.R., Vang Hendriksen, P., Münster, M., 2023. Techno-economic assessment of green ammonia production with different wind and solar potentials. *Renew. Sustain. Energy Rev.* 173, 113057. <http://dx.doi.org/10.1016/j.rser.2022.113057>, URL <https://www.sciencedirect.com/science/article/pii/S1364032122009388>.
- ChemAnalyst, 2023. Nitric acid price trend and forecast. URL <https://www.chemanalyst.com/Pricing-data/nitric-acid-1142>.
- Christensen, P., Dysert, L., Bates, J., Burton, D., Creese, R., Hollmann, J., et al., 2005. Cost estimate classification system-as applied in engineering, procurement, and construction for the process industries. In: AACE International Recommended Practices. pp. 1–30.
- Ciccarelli, G., Jackson, D., Verreault, J., 2006. Flammability limits of NH₃-H₂-N₂-air mixtures at elevated initial temperatures. *Combust. Flame* 144 (1), 53–63. <http://dx.doi.org/10.1016/j.combustflame.2005.06.010>, URL <https://www.sciencedirect.com/science/article/pii/S0010218005001744>.
- Clarke, S.I., Mazzafro, W.J., Updated by Staff, 2005. Nitric acid. In: Kirk-Othmer Encyclopedia of Chemical Technology. John Wiley & Sons, Ltd, <http://dx.doi.org/10.1002/0471238961.1409201803120118.a01.pub2>, URL <https://onlinelibrary.wiley.com/doi/abs/10.1002/0471238961.1409201803120118.a01.pub2>.
- Dersch, J., Dieckmann, S., Hennecke, K., Pitz-Paal, R., Taylor, M., Ralon, P., 2020. LCOE reduction potential of parabolic trough and solar tower technology in G20 countries until 2030. In: AIP Conference Proceedings. Vol. 2303. American Institute of Physics Inc.
- Echegaray, D., Velloso, A., Wagner, M., 2000. Method and production of nitric acid. US Patent 6165435A.
- Elkin, E., 2021. Fertilizer prices rocket to all-time high on tightening supplies. URL <https://www.bloomberg.com/news/articles/2021-11-12/fertilizer-prices-rocket-to-new-record-for-second-week?leadSource=verify%20wall>.
- European Central Bank, 2023. URL https://www.ecb.europa.eu/stats/policy_and_exchange_rates/euro_reference_exchange_rates/html/eurofxref-graph-usd.en.html.
- European Parliament and Council, 2023. Establishing a system for greenhouse gas emission allowance trading within the union and amending council: Directive 2003/87/EC. URL <http://data.europa.eu/eli/dir/2003/87/2023-03-01>.
- Gamarrá, A., Banacloche, S., Lechon, Y., del Río, P., 2023. Assessing the sustainability impacts of concentrated solar power deployment in Europe in the context of global value chains. *Renew. Sustain. Energy Rev.* 171, 113004. <http://dx.doi.org/10.1016/j.rser.2022.113004>, URL <https://www.sciencedirect.com/science/article/pii/S1364032122008851>.
- Global petrol prices, 2022. Spain electricity prices. URL https://www.globalpetrolprices.com/Spain/electricity_prices/#hl223.
- Goodwin, D.G., Moffat, H.K., Schoegl, I., Speth, R.L., Weber, B.W., 2022. Cantera: An object-oriented software toolkit for chemical kinetics, thermodynamics, and transport processes. <http://dx.doi.org/10.5281/zenodo.6387882>, Version 2.6.0, <https://www.cantera.org>.
- Grande, C., Andreassen, K., Cavka, J., Waller, D., Lorentsen, O., Øien, H., Zander, H., Poulston, S., García, S., Modeshia, D., 2018. Process intensification in nitric acid plants by catalytic oxidation of nitric oxide. *Ind. Eng. Chem. Res.* 57 (31), 10180–10186. <http://dx.doi.org/10.1021/acs.iecr.8b01483>.
- Groves, M.C., 2000. Nitric acid. In: M. C. E. Kirk-Othmer Encyclopedia of Chemical Technology, 1st ed. John Wiley & Sons, Inc, pp. 1–37. <http://dx.doi.org/10.1002/0471238961.1409201803120118.a01.pub3>.
- Haar, L., Gallagher, J.S., Kell, G.S., 1984. NBS/NRC steam tables thermodynamic and transport properties and computer programs for vapor and liquid states of water in SI units, URL <https://www.osti.gov/biblio/5614915>.
- Hacker, V., Kordesch, K., 2003. Ammonia crackers / ammoniak cracker. In: Handbook of Fuel Cells – Fundamentals, Technology and Applications. Vol. 3. John Wiley & Sons, pp. 121–127.
- Harris, G., MacDermott, P., 1977. Flammability and explosibility of ammonia. In: IChemE Symposium Series. Vol. 49.
- Haynes, B.S., 2019. Combustion research for chemical processing. *Proc. Combust. Inst.* 37 (1), 1–32. <http://dx.doi.org/10.1016/j.proci.2018.06.183>, URL <https://www.sciencedirect.com/science/article/pii/S1540748918303699>.
- Il'chenko, N.I., 1976. Catalytic oxidation of ammonia. *Russ. Chem. Rev.* 45 (12), 1119. <http://dx.doi.org/10.1070/RC1976v045n12ABEH002765>.
- Kamphus, M., 2014. Emission monitoring in nitric acid plants. *Nitrogen+Syngas* 328 (2), 48–53.
- Klaas, L., Bulfin, B., Kriechbaumer, D., Neumann, N., Roeb, M., Sattler, C., 2023. Energetic optimization of thermochemical air separation for the production of sustainable nitrogen. *React. Chem. Eng.* <http://dx.doi.org/10.1039/D3RE00087G>.
- Kniel, G., Delmarco, K., Petrie, J., 1996. Life cycle assessment applied to process design: Environmental and economic analysis and optimization of a nitric acid plant. *Environ. Prog.* 15 (4), 221–228. <http://dx.doi.org/10.1002/ep.670150410>, URL <https://aiche.onlinelibrary.wiley.com/doi/abs/10.1002/ep.670150410>.
- Koukolik, M., Marek, J., 1968. Mathematical model of HNO₃ oxidation—absorption equipment. In: Proc. of the Fourth European Symp. on Chem. React. Eng. pp. 347–359.
- Lee, B., Winter, L.R., Lee, H., Lim, D., Lim, H., Elimelech, M., 2022. Pathways to a green ammonia future. *ACS Energy Lett.* 7 (9), 3032–3038. <http://dx.doi.org/10.1021/acsenerylett.2c01615>.

- Li, Y., Bi, M., Zhang, K., Gao, W., 2021. Effects of nitrogen and argon on ammonia-oxygen explosion. *Int. J. Hydrogen Energy* 46 (40), 21249–21259. <http://dx.doi.org/10.1016/j.ijhydene.2021.03.212>, URL <https://www.sciencedirect.com/science/article/pii/S0360319921011915>.
- Liu, Y., Han, D., 2021. Numerical study on explosion limits of ammonia/hydrogen/oxygen mixtures: Sensitivity and eigenvalue analysis. *Fuel* 300, 120964. <http://dx.doi.org/10.1016/j.fuel.2021.120964>, URL <https://www.sciencedirect.com/science/article/pii/S0016236121008413>.
- Maxwell, C., 2023. URL <https://toweringskills.com/financial-analysis/cost-indices/>.
- Mei, B., Zhang, X., Ma, S., Cui, M., Guo, H., Cao, Z., Li, Y., 2019. Experimental and kinetic modeling investigation on the laminar flame propagation of ammonia under oxygen enrichment and elevated pressure conditions. *Combust. Flame* 210, 236–246. <http://dx.doi.org/10.1016/j.combustflame.2019.08.033>, URL <https://www.sciencedirect.com/science/article/pii/S0010218019303979>.
- Menegat, S., Ledo, A., Tirado, R., 2022. Greenhouse gas emissions from global production and use of nitrogen synthetic fertilisers in agriculture. *Sci. Rep.* 12 (1), 14490. <http://dx.doi.org/10.1038/s41598-022-18773-w>.
- Miller, D., 1987. Mass transfer in nitric acid absorption. *AIChE J.* 33 (8), 1351–1358. <http://dx.doi.org/10.1002/aic.690330812>, URL <https://aiche.onlinelibrary.wiley.com/doi/abs/10.1002/aic.690330812>.
- Mock, B., Evans, L., Chen, C.-C., 1986. Thermodynamic representation of phase equilibria of mixed-solvent electrolyte systems. *AIChE J.* 32 (10), 1655–1664. <http://dx.doi.org/10.1002/aic.690321009>, URL <https://aiche.onlinelibrary.wiley.com/doi/abs/10.1002/aic.690321009>.
- Moghaddam, A., Krewer, U., 2020. Poisoning of ammonia synthesis catalyst considering off-design feed compositions. *Catalysts* 10 (1225), 1–16. <http://dx.doi.org/10.3390/catal10111225>, URL <https://www.mdpi.com/2073-4344/10/11/1225>.
- Peters, M., Timmerhaus, K., West, R., 2003. *Plant Design and Economics for Chemical Engineers*, 5th ed. McGrawHill.
- Powell, J., 1975. Process for making nitric acid by the ammonia oxidation-nitric oxide oxidation-water absorption method. US Patent 3927182A.
- PwC-Spain, 2023. Worldwide tax summaries. URL <https://taxsummaries.pwc.com/spain/corporate/withholding-taxes>.
- Randive, K., Raut, T., Jawadand, S., 2021. An overview of the global fertilizer trends and India's position in 2020. *Miner. Econ.* 34, 371–384. <http://dx.doi.org/10.1007/s13563-020-00246-z>, URL <https://link.springer.com/article/10.1007/s13563-020-00246-z>.
- Rehman, A., Saleem, A., Hussain, S., Yousf, M., Ayub, A., Afzal, M., 2007. Production of 140 MTPD Conc. Nitric Acid (98%) by Recycling and Rectification. Technical Report, NFC Institute of Engineering & Fertilizer Research.
- Rosenstiel, A., Monnerie, N., Dersch, J., Roeb, M., Pitz-paal, R., Sattler, C., 2021. Electrochemical hydrogen production powered by PV/CSP hybrid power plants: A modelling approach for cost optimal system design. *Energies* 2021 14 (12), <http://dx.doi.org/10.3390/en14123437>, URL <https://www.mdpi.com/1996-1073/14/12/3437>.
- Schwartz, S.E., White, W.H., 1981. Solubility equilibria of the nitrogen oxides and oxyacids in dilute aqueous solution. *Adv. Environ. Sci. Eng.; (United States)* 4, URL <https://www.osti.gov/biblio/6439659>.
- Selectra, 2022. Precio de agua en españa: Toda la información. URL <https://tarifasdeagua.es/info/precio>.
- Smil, V., 2004. *Enriching the Earth: Fritz Haber, Carl Bosch, and the Transformation of World Food Production*. Massachusetts Institute of Technology Press.
- Sperner, F., Hohmann, W., 1976. Rhodium-platinum gauzes for ammonia oxidation. *Platinum Metals Rev.* 20 (1), 12–20, URL <https://www.ingentaconnect.com/content/matthey/pmr/1976/00000020/00000001/art00007>.
- Suchak, N., Joshi, J., 1994. Simulation and optimization of NOx absorption system in nitric acid manufacture. *AIChE J.* 40 (6), 944–956. <http://dx.doi.org/10.1002/aic.690400605>, URL <https://aiche.onlinelibrary.wiley.com/doi/abs/10.1002/aic.690400605>.
- Thiemann, M., Scheibler, E., Wiegand, K., 2000. Nitric acid, nitrous acid, and nitrogen oxides. In: *Ullmann's Encyclopedia of Industrial Chemistry*. Wiley-VCH Verlag GmbH & Co. KGaA.
- Trading Economics, 2023. URL <https://tradingeconomics.com/commodity/carbon>.
- Vatavuk, W.M., et al., 2002. Updating the CE plant cost index. *Chem. Eng.* 109 (1), 62–70.
- Vieten, J., Gubán, D., Roeb, M., Lachmann, B., Richter, S., Sattler, C., 2020. Ammonia and nitrogen-based fertilizer production by solar-thermochemical processes. *AIP Conf. Proc.* 2303 (1), <http://dx.doi.org/10.1063/5.0030980>, 170016.
- Wagner, M., Plains, W., 2003. Direct oxygen injection in nitric acid production. European Patent 0808797A3.
- Watson, R., Balkey, P., 1980. Oxygen-enrichment columnar absorption process for making nitric acid. US Patent 4183906.
- Wernet, G., Bauer, C., Steubing, B., Reinhardt, J., Moreno-Ruiz, E., Weidema, B., 2016. The ecoinvent database version 3 (part I): Overview and methodology. *ecoinvent database version 3.7.1, cut-off*. *Int. J. Life Cycle Assess.* 21, 1218–1230. <http://dx.doi.org/10.1007/s11367-016-1087-8>, URL <http://link.springer.com/10.1007/s11367-016-1087-8>.
- Xin, L., Yongqiang, H., Husheng, J., 2017. Pt-Rh-Pd alloy group Gauze catalysts used for ammonia oxidation. *Rare Metal Mater. Eng.* 46 (2), 339–343. [http://dx.doi.org/10.1016/S1875-5372\(17\)30091-7](http://dx.doi.org/10.1016/S1875-5372(17)30091-7), URL <https://www.sciencedirect.com/science/article/pii/S1875537217300917>.